Influence of the Charge at D85 on the Initial Steps in the Photocycle of Bacteriorhodopsin

Constanze Sobotta,[†‡] Markus Braun,[†‡*] Jörg Tittor,[§] D. Oesterhelt,[§] and Wolfgang Zinth[†‡]
[†]Lehrstuhl für BioMolekulare Optik, Fakultät für Physik, Ludwig-Maximilians-Universität München, and [‡]Center For Integrated Protein Science Munich (CIPSM), Munich, Germany; and [§]Max-Planck-Institut für Biochemie, Martinsried, Germany

ABSTRACT Studies have shown that *trans-cis* isomerization of retinal is the primary photoreaction in the photocycle of the light-driven proton pump bacteriorhodopsin (BR) from *Halobacterium salinarum*, as well as in the photocycle of the chloride pump halorhodopsin (HR). The transmembrane proteins HR and BR show extensive structural similarities, but differ in the electrostatic surroundings of the retinal chromophore near the protonated Schiff base. Point mutation of BR of the negatively charged aspartate D85 to a threonine T (D85T) in combination with variation of the pH value and anion concentration is used to study the ultrafast photoisomerization of BR and HR for well-defined electrostatic surroundings of the retinal chromophore. Variations of the pH value and salt concentration allow a switch in the isomerization dynamics of the BR mutant D85T between BR-like and HR-like behaviors. At low salt concentrations or a high pH value (pH 8), the mutant D85T shows a biexponential initial reaction similar to that of HR. The combination of high salt concentration and a low pH value (pH 6) leads to a subpopulation of 25% of the mutant D85T whose stationary and dynamic absorption properties are similar to those of native BR. In this sample, the combination of low pH and high salt concentration reestablishes the electrostatic surroundings originally present in native BR, but only a minor fraction of the D85T molecules have the charge located exactly at the position required for the BR-like fast isomerization reaction. The results suggest that the electrostatics in the native BR protein is optimized by evolution. The accurate location of the fixed charge at the aspartate D85 near the Schiff base in BR is essential for the high efficiency of the primary reaction.

INTRODUCTION

The native environment of the archaeon *Halobacterium salinarum* consists of saturated salt brines under conditions of strong illumination (1–5). The metabolism of the archeon depends on its specific location in that environment. When it is close to the surface, where the oxygen concentration is sufficiently high, the archeon lives from respiration. Under anoxygenic conditions, *H. salinarum* switches to phototrophic growth and uses different retinal proteins. The membrane of the *Halobacterium* is functionalized by four light-driven transmembrane proteins: bacteriorhodopsin (BR, proton pump), halorhodopsin (HR, chloride pump), and two sensory rhodopsins (SR I and SR II). All of these proteins exert their functions via the photoisomerization properties of their chromophore retinal, which is bound to the protein via a Schiff base (6–9). In the four proteins the ultrafast photoisomerization of retinal as the primary reaction initiates different functions: BR—proton transport to the extracellular side of the membrane, generating an electrochemical gradient (photosynthesis) (10,11); HR—a chloride anion is pumped into the cytoplasm to provide isoosmotic pressure conditions (12,13); and SRI and SRII—signal transmission initiated by absorption of visible or UV light used in phototaxis (14–18). The overall structures of BR and HR are similar (19–23). Both contain seven transmembrane helices, and the sequences of the two proteins show a strong homology (24–30). The functionality of BR and HR is highly dependent on the specific amino acids. For example, studies have shown that a single point mutation at residue D85, together with adjustments of the pH value, the salt concentration, or the illumination condition, can switch the ion transport capability of BR from proton-outward pumping to proton-inward pumping or to chloride-inward pumping (31–33). Thus, the functionality of BR can be switched to an HR-like behavior because of the substitution of the charged aspartate D85 by the neutral threonine (T) in the vicinity of the Schiff base of the retinal (mutant BR-D85T). In those studies, threonine was chosen for that specific mutant because a threonine is found at the equivalent position in HR. Since aspartate (D) and threonine occupy a similar volume in the protein, this choice should minimize structural changes upon mutation (Fig. 1). This assumption is supported by x-ray diffraction results from a similar BR mutant D85S (34,35). The most prominent modification by this mutation is expected to be an altered electrostatic environment around the retinal. Under physiological conditions (pH ranging from 4 to 12), the aspartate residue D85 of BR is negatively charged. At high pH conditions (pH $>$ 7), the anion-binding sites of mutant BR-D85T and HR (where a threonine residue is located at the corresponding position T111) are similar and uncharged because of the neutral hydroxyl moiety in threonine.

After optical excitation, the photoreactions of HR and the BR mutant D85T show similar microsecond reaction dynamics. However, the anion transport of the natural anion pump HR is 10-fold more efficient (36). It was shown (33) that one can shift the peak of the steady-state absorption by varying the pH value and the salt concentration. This

Submitted September 22, 2008, and accepted for publication April 6, 2009.

*Correspondence: markus.braun@physik.uni-muenchen.de

Editor: Janos K. Lanyi.

0006-3495/09/07/0267/10 $2.00

doi: 10.1016/j.bpj.2009.04.021

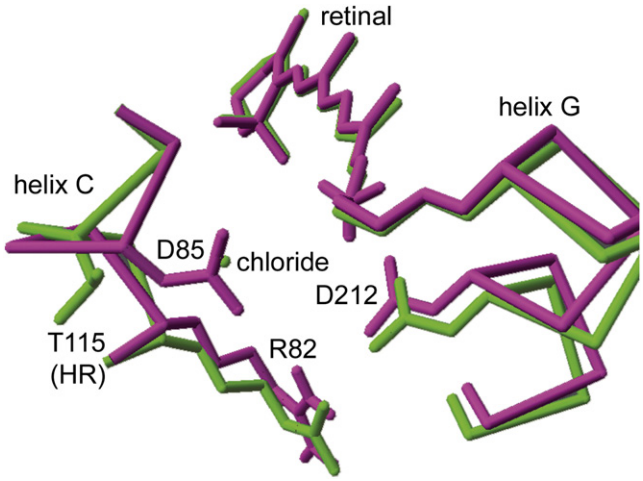

FIGURE 1 Detailed view of the environment around the protonated Schiff bases in BR (*red*) and HR (*green*). The two structures were overlaid to minimize the root mean-square of the Ca atoms of the total proteins. For clarity, only part of helices C and G are shown, as well as the side chains of D85 and R82 (nomenclature of BR) and T111 (HR), and D212 and K216 of BR, with their corresponding residues in HR. The chloride ion in the HR structure (*green sphere*) is at exactly the same position as the carboxylic group of the D85 side chain in the BR structure. (The figure was prepared using Swiss-PdbViewer public domain software.)

indicates that the electrostatic environment of the Schiff base of the retinal chromophore depends on these parameters. These observations argue for an extended experimental study of the primary dynamics of the three samples (BR, BR-D85T, and HR).

In the following, we will summarize published information on the primary reaction steps of the photocycle in the femtosecond and picosecond range for HR and BR. The charge transport is initiated by the retinal photoisomerization from all-*trans* to the 13-*cis* form for both HR and BR. The essential processes in the ultrafast dynamics of BR can be described by the sequence of intermediates:

$$\mathrm{BR} \xrightarrow{h\nu} \mathrm{BR^{*}FC} \xrightarrow{\sim 200\ \mathrm{fs}} \mathrm{BR^{*}} \xrightarrow{450\ \mathrm{fs}} \mathrm{J_{625}} \xrightarrow{3-5\ \mathrm{ps}} \mathrm{K_{590}}$$

After photoexcitation of all-*trans* retinal, one finds a movement out of the Franck-Condon region on the <200 fs timescale, which may be connected to pronounced wave packet-like motions on the excited-state potential energy surface (37–40). The excited state decays with a time constant of 450 fs to a hot ground state (J_{625}) in a distorted 13-*cis* form. The relaxed 13-*cis* photoproduct K_{590} is reached after ~3–5 ps (37,41–43). After formation of the K_{590} photoproduct, slower dynamics occur in the range of several nanoseconds and are followed by proton transfer in the microsecond range from the Schiff base to the aspartate residue D85. The aspartate D85 acts as primary proton acceptor at the extracellular side of the protein (44–47). The primary steps leading to the isomerization of the retinal chromophore on the (sub-) picosecond timescale are separated in time by more than three orders of magnitude from the processes directly related to the proton transfer.

The primary reaction dynamics observed after photoexcitation of all-*trans* retinal in HR involve slower processes. A biexponential (1.5 and 8.5 ps) decay of the excited state to a 13-*cis* ground state is observed (48–52). A model for the early steps of the photocycle of HR was proposed by Arlt et al. (50): After photoexcitation of HR to the excited-state HR*, two intermediate excited states are populated within 170 fs. These intermediate excited states decay with time constants of 1.5 and 8.5 ps, and the 13-*cis* photoproduct is formed. This reaction pathway was recently confirmed by transient infrared (IR) experiments (49). In that study it was found that one intermediate decays with a time constant of 8.5 ps back to the *trans*-HR ground state, whereas the other intermediate state undergoes *trans-cis* isomerization. The 13-*cis*-HR ground state HR_{600} is formed with a time constant of 1.5 ps. The transport of the chloride anion to the cytoplasmic side takes place after the isomerization via several long-lived intermediates in a time range of several microseconds.

In earlier studies, the initial reaction steps in HR were investigated only at low salt concentration (100 mM NaCl), well below the physiological conditions of *H. salinarum* (50). To date, the photoreactions of the BR mutant D85T have only been characterized by transient absorption spectroscopy in the visible range of the spectrum with a millisecond time resolution (33). These experiments covered the long-lived intermediates in the photocycle that account for the ion transport processes and are similar to the chloride transport of wild-type HR. The influence of the point mutation D85T on the initial dynamics (in particular, the isomerization of the retinal) is not known.

In this work, we performed femtosecond, time-resolved, transient absorption experiments on HR and the mutant D85T at different pH values and salt concentrations. Care was taken to perform the experiments on wild-type HR and the mutant BR-D85T under conditions close to those found in the cell under native conditions (e.g., low sample concentration and protein bound in purple membrane). The results provide new information about the role of the chloride counterion in the primary reaction dynamics, and have implications for our understanding of the counterion in wild-type BR and ultrafast isomerization dynamics.

MATERIALS AND METHODS

The femtosecond transient absorption experiments were performed using a setup based on an in-house-built Ti:sapphire laser chirped pulse amplifier (CPA) system with a repetition rate of 1 kHz, as described in detail elsewhere (53). One part of the Ti:sapphire amplifier operating at a central wavelength of 800 nm pumps a double-stage noncollinear optical parametric amplifier (NOPA) that provides excitation pulses between 570 and 610 nm. These pulses were compressed to a pulse duration of 100 fs (full width at half-maximum (FWHM)) via a prism compressor and focused onto a fused silica sample cell with an optical path length of 0.5 mm. The excitation light energy densities were kept low enough to obtain a linear response from the sample (54). Another part of the CPA output generated a white light continuum for the probe pulses using a CaF_2 plate (55). The polarization

TABLE 1 Properties of the investigated samples (buffer, pH value, salt concentration, and absorption)

Sample	Buffer	pH Value	Salt concentration	λ max
BR	20 mM KPO_4	7.5	150 mM KCl	568 nm
HR	50 mM MOPS	7.5	no salt added	578 nm
HR	50 mM MOPS	7.5	4 M NaCl	578 nm
D85T	50 mM TRIS (HCl)	8.0	no salt added	616 nm
D85T	50 mM TRIS (HCl)	8.0	1 M NaCl	617 nm
D85T	60 mM NaPi (NaOH)	6.0	no salt added	615 nm
D85T	60 mM NaPi (NaOH)	6.0	1 M NaCl	570 nm

of the probe light was at the magic angle relative to the excitation pulses. The absorbance changes were detected with a multichannel detector that allowed broadband probing ranging from 430 to 760 nm (56). The sample volume was completely exchanged between two laser shots.

Isolation of BR from cells was carried out according to the standard procedure (57). After lysis of the cells in the presence of DNase I (Sigma, Steinheim, Germany), the resultant membrane fragments were washed with water and then purified by centrifugation on a sucrose gradient (25–45% w/w). Membrane fractions of buoyant density 1.18 g/mL were collected, washed repeatedly with water, and then resuspended in the appropriate buffer solution (pH 7.5) for spectroscopic measurements. The samples were light-adapted for at least 30 min before the measurements were obtained, and circulated through fused silica flow cells with an optical path length of 0.5 mm.

HR from *H. salinarum* strain D2 was prepared in a membrane-bound form as described previously (58). In this study we did not use the lowest band from a sucrose gradient (25–45%); rather, we used the one next to it. This band, which contained 80–90% of the total expressed HR, was isolated and washed two times and resuspended in 50 mM MOPS buffer (3-(*N*-morpholino)propanesulfonic acid) at pH 7.5 either without salt or 4 M NaCl added.

BR mutant D85T was prepared by means of site-directed polymerase chain reaction (PCR) mutagenesis by overlap extension as described previously (59). The PCR product was cloned in the shuttle vector pUS-Mev. Mutagenesis was followed by transformation and homologous expression in *H. salinarum* strain SNOB, a bacterioopsin deletion strain (59).

Membrane suspensions containing 5 nmol of the chromoprotein were mixed with an equal volume of isopropanol to denaturate the protein. Sodium phosphate buffer pH 7.0 was added to obtain a final concentration of 100 mM. Extraction of retinal was performed by addition of 1.5 volumes of hexane (two times). The organic phase was dried from residual water by treatment with Na_2SO_4. The volume of hexane was reduced to 100 mL and injected into a high-performance liquid chromatography system with a Lichrosorb 60 column and retinals eluted with 5% ethylacetate in hexane. All-*trans* and 13-*cis* retinal were identified by comparison with extractions from wild-type purple membranes, and 9-*cis* retinal was identified by the retention time and by the fact that the extracted proportion increased by shifting the illumination wavelength to the red (60).

The relevant parameters for the investigated samples of BR, HR, and the BR mutant D85T are summarized in Table 1.

RESULTS

Steady-state absorption

HR samples were investigated in aqueous solution with NaCl concentration $c_{NaCl} = 4.0$ M and also without NaCl. The BR mutant D85T was investigated under four different conditions: low salt, $c_{NaCl} = 0$ M and pH = 6.0 (sample $D85T_{low\ salt,\ pH\ 6}$); high salt, $c_{NaCl} = 1$ M and pH = 6.0 (sample $D85T_{high\ salt,\ pH\ 6}$); low salt, $c_{NaCl} = 0$ M and pH = 8.0 (sample $D85T_{low\ salt,\ pH\ 8}$); and high salt, $c_{NaCl} = 1$ M and pH = 8.0 (sample $D85T_{high\ salt,\ pH\ 8}$).

The steady-state absorption spectra of the two HR samples are presented in Fig. 2 *a*. For HR the absorption maximum is located at 578 nm. The spectral shape and the spectral position of the absorption are independent of the NaCl concentration. The sample without NaCl shows a reduced scattering background and noise level.

In Fig. 2 *b* the absorption spectra of the four D85T samples (*solid lines*) and wild-type BR (*broken line*) as reference are presented. The absorption maximum of wild-type BR is observed at 568 nm. The absorption spectra of the mutant D85T strongly deviate from those of wild-type BR. In addition, they depend on the pH value and NaCl concentration (33). The samples $D85T_{low\ salt,\ pH\ 8}$, $D85T_{high\ salt,\ pH\ 8}$, and $D85T_{low\ salt,\ pH\ 6}$ show the same spectral behavior in the red spectral range, with an absorption maximum around 615 nm. Only in a spectral range below 500 nm can differences be observed in their absorption spectra, which may be related

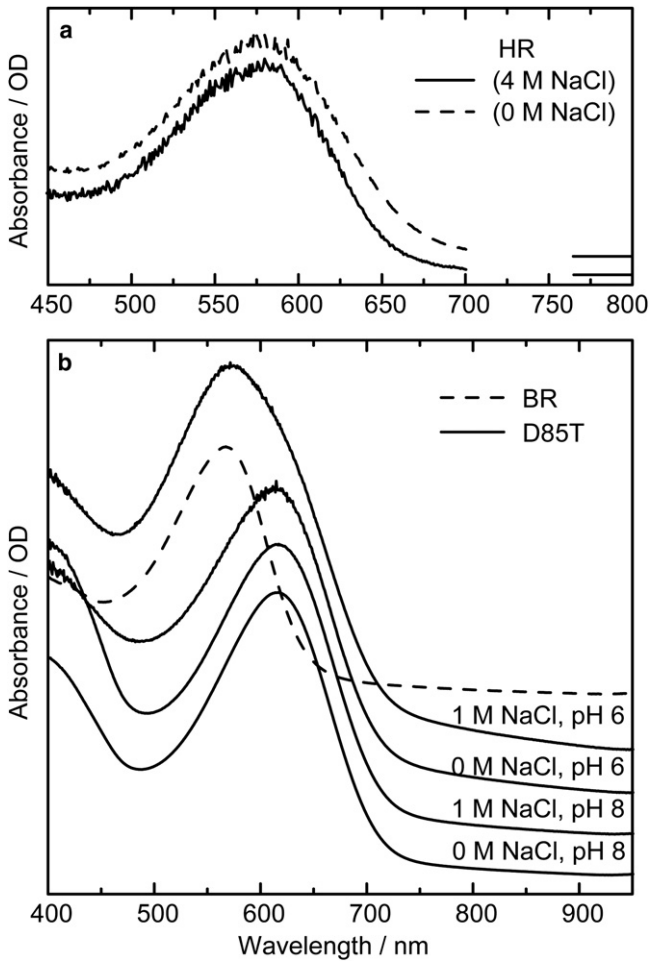

FIGURE 2 Steady-state absorption spectra of the investigated samples. (*a*) HR dissolved in 50 mM MOPS buffer at pH 7.5 with no salt (0 M NaCl) or 4 M NaCl added. (*b*) BR wild-type (*broken line*) and mutant BR-D85T (*line*) with different pH values and salt concentrations (as indicated in the graph).

to differences in the scattering background. The sample $D85T_{high\ salt,\ pH\ 6}$ differs from all other samples by having a strongly broadened absorption spectrum, with the absorption peak at 570 nm and a distinct shoulder extending into the red.

Transient absorption dynamics

HR at different salt concentrations

Fig. 3 shows an overview of the transient absorption changes for HR with high (4 M) NaCl concentration and without NaCl. The wavelength for optical excitation was chosen to be 575 nm. A first inspection of the experimental data shows that both HR samples behave in a very similar way (Fig. 3). The population of the electronically excited state is seen via an instantaneous rise of the stimulated emission signal at 650 nm and the induced absorption signal around 500 nm. On the timescale of 100 fs, there are initial excited-state relaxation processes followed by a biphasic decay of excited-state absorption and stimulated emission on the timescale of a few picoseconds. Subsequently, a red-shifted state with increased absorption around 650 nm and bleaching around 570 nm is formed with spectral signatures characteristic of the HR_k reaction intermediate. It should be noted that the overall features—femtosecond excited-state dynamics, biphasic decay of the electronic state, and absorption spectra of the intermediates—are very similar for both samples. One may conclude that the large difference in NaCl concentration (0 M vs. 4 M) does not influence the general features of the initial reaction dynamics of HR.

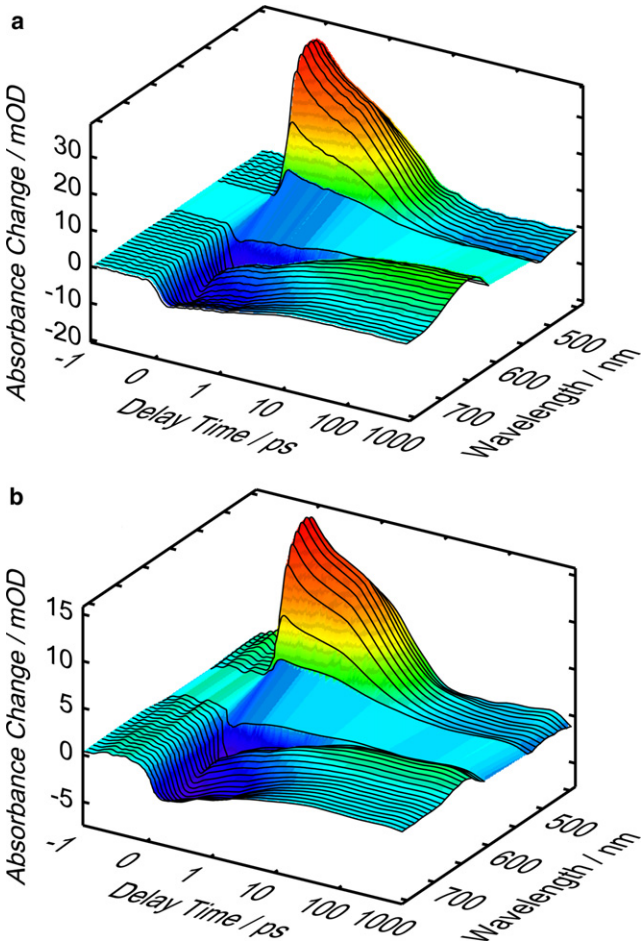

FIGURE 3 Transient absorption spectra for HR with (*a*) no (0 M) and (*b*) high (4 M) NaCl concentration excited at 575 nm. The delay time between −1 ps and 1 ps is plotted on a linear axis and, for longer delay times, on a logarithmic axis. The ultrafast dynamics of both HR samples is not influenced by the salt concentration.

TABLE 2 Time constants of the dynamics for HR

	t_1/[ps]	t_2/[ps]	t_3/[ps]	t_4/[ps]
HR (4M NaCl)	0.1 (33%)	1.0 (33%)	5.2 (37%)	offset (−3%)
HR (without NaCl)	0.1 (31%)	1.4 (42%)	8.1 (31%)	offset (−4%)

The values in brackets give the relative amplitudes of the respective decay components for the probe wavelength at 500 nm.

A more detailed analysis of the transient absorption data also suggests a high similarity between the samples. The time constants determined in a global fitting procedure are displayed in Table 2, which shows only small differences between the two samples. The spectral features connected with the various time constants do not exhibit pronounced differences. The decay-associated difference spectra of the HR sample with low salt concentration (which were recorded with a better signal/noise ratio because of the lower-scattering background) are presented in Fig. 4. These spectra are very similar to those published previously (50).

Absorption dynamics of the BR mutant D85T

For the D85T mutant, transient absorption data were recorded under four different sample conditions (two pH values and two different salt concentrations). The transient absorption data of all four samples were recorded under identical experimental conditions. Qualitatively, an inspection of the transient absorption changes reveals that the three samples ($D85T_{low\ salt,\ pH\ 8}$, $D85T_{high\ salt,\ pH\ 8}$, and $D85T_{low\ salt,\ pH\ 6}$) show nearly identical results. It should be noted that these three samples also exhibit very similar stationary absorption spectra. In addition, these three samples qualitatively show transient behavior identical to that described above for HR: after the initial excited-state dynamics, biexponential picosecond transients lead to a red-shifted photoproduct. The two picosecond time constants are somewhat longer than those observed for HR (Tables 2 and 3).

The transient absorption changes in the $D85T_{high\ salt,\ pH\ 6}$ sample deviate significantly from those of the other D85T samples. Pronounced differences during the first picosecond indicate that an additional fast reaction process is present in the $D85T_{high\ salt,\ pH\ 6}$ system. Analysis of the data with a multiexponential global fitting procedure assigns a 0.5 ps kinetic constant to this additional process (Table 3). This additional fast decay component can be seen directly in the

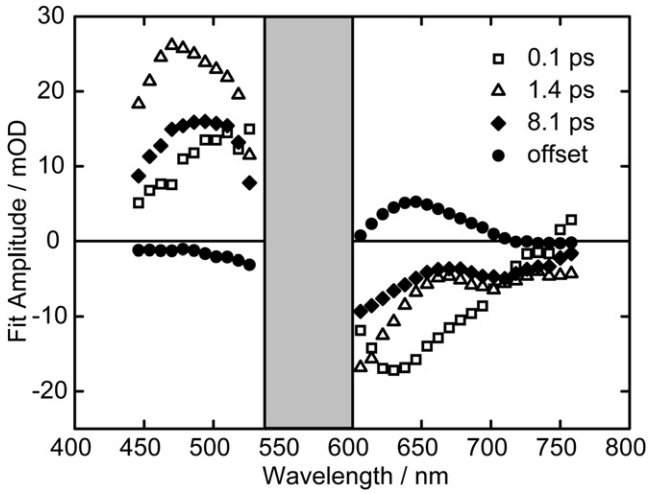

FIGURE 4 Decay-associated difference spectra of HR (0 M NaCl) for the time constants 0.1 ps, 1.4 ps, and 8.1 ps. The offset spectrum accounts for long-lived intermediates in the photocycle. Because of scattering of the pump pulse, the gray shaded part of the transient spectrum around 575 nm is not shown.

experimental data when one compares signal traces from the two $D85T_{low\ salt,\ pH\ 6}$ and $D85T_{high\ salt,\ pH\ 6}$ samples in the spectral ranges of induced absorption and stimulated emission (Fig. 5). The concentration of the $D85T_{low\ salt,\ pH\ 6}$ and $D85T_{high\ salt,\ pH\ 6}$ samples was adjusted to obtain an identical number of excited molecules because of the pump pulse. At later delay times ($t_D > 1$ ps), the induced absorption signals of the two samples for the probe wavelength of 510 nm (Fig. 5 *a*) behave very similarly, apart from a constant scaling factor. For shorter delay times, however, an additional fast 0.5 ps component is clearly seen for the $D85T_{high\ salt,\ pH\ 6}$ sample. A similar observation is made for the decay of the stimulated emission signal at 678 nm (Fig. 5 *b*), where an additional ultrafast change in signal amplitude shows up.

In Fig. 6 the decay-associated spectra for the $D85T_{low\ salt,\ pH\ 6}$, $D85T_{high\ salt,\ pH\ 6}$, and BR samples are compared. The decay-associated spectra for the $D85T_{high\ salt,\ pH\ 6}$ sample are presented on the right-hand side for the time constants 0.5 ps, 3 ps, and 12 ps, as obtained from the global fitting procedure. The global fit yields time constants of 3 ps and 12 ps for the $D85T_{low\ salt,\ pH\ 6}$ sample, and 0.5 ps and 3 ps for the BR sample. The respective fit amplitudes are shown on the left-hand side. The decay-associated spectra for BR are plotted with scaled amplitude by a factor of 0.25. Fig. 6 clearly shows that the decay-associated spectra of

TABLE 3 Time constants of the BR mutant D85T

	t_1/[ps]	t_2/[ps]	t_3/[ps]	t_4/[ps]	t_5/[ps]
$D85T_{low\ salt,\ pH\ 8}$	0.1 (18%)	— (0%)	3.1 (35%)	14.9 (47%)	offset
$D85T_{high\ salt,\ pH\ 8}$	0.1 (13%)	— (0%)	2.4 (37%)	11.9 (50%)	offset
$D85T_{low\ salt,\ pH\ 6}$	0.1 (12%)	— (0%)	2.5 (28%)	12.6 (60%)	offset
$D85T_{high\ salt,\ pH\ 6}$	0.2 (9%)	0.5 (12%)	4.0 (59%)	16.8 (20%)	offset

The values in brackets give the relative amplitudes of the respective decay components for the probe wavelength at 500 nm.

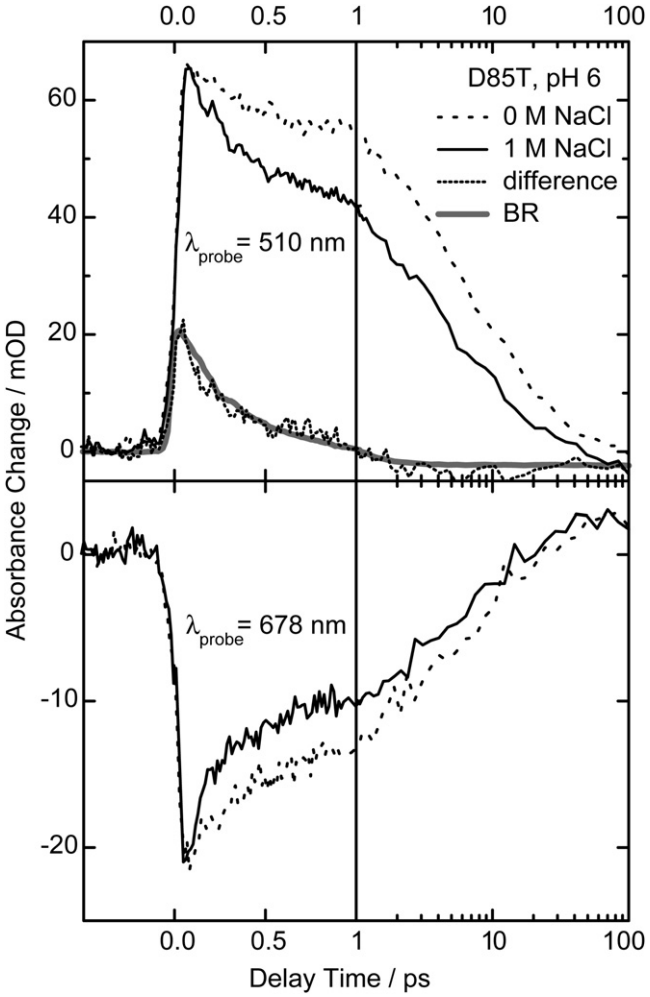

FIGURE 5 Transient absorption signal for the BR mutants $D85T_{high\ salt,\ pH\ 6}$ (*line*) and $D85T_{low\ salt,\ pH\ 6}$ (*broken line*) at a probe wavelength of 510 nm (*upper panel*) and 678 nm (*lower panel*). The difference spectrum (*dotted line*) is calculated according to ($A(D85T_{high\ salt,\ pH\ 6}) - 0.75 \times A(D85T_{low\ salt,\ pH\ 6})$). For comparison, the transient signal of wild-type BR (*gray line*) is shown (scaled by a factor of 0.25).

the 0.5 ps component of BR and $D85T_{high\ salt,\ pH\ 6}$ are very similar. In addition, the decay-associated spectra for the long time constant of ~12 ps in the two mutant samples $D85T_{low\ salt,\ pH\ 6}$ and $D85T_{high\ salt,\ pH\ 6}$ display a similar behavior. For the 3-ps component, some differences in the decay-associated spectra can be observed in the red spectral range between 600 and 750 nm for the $D85T_{low\ salt,\ pH\ 6}$ and $D85T_{high\ salt,\ pH\ 6}$ samples.

An inspection of the decay-associated spectra (Fig. 6) and the transient data (Fig. 5) suggests that the $D85T_{high\ salt,\ pH\ 6}$ sample exhibits, to a certain extent, a BR-like behavior (37,43). This can be seen when the differences in the transient absorption changes of the $D85T_{low\ salt,\ pH\ 6}$ and $D85T_{high\ salt,\ pH\ 6}$ samples are calculated (*dotted line* in Fig. 5 *a*). This difference is very similar to the gray curve, which is the transient absorption signal of wild-type BR at the same probing wavelength scaled by a factor of 0.25.

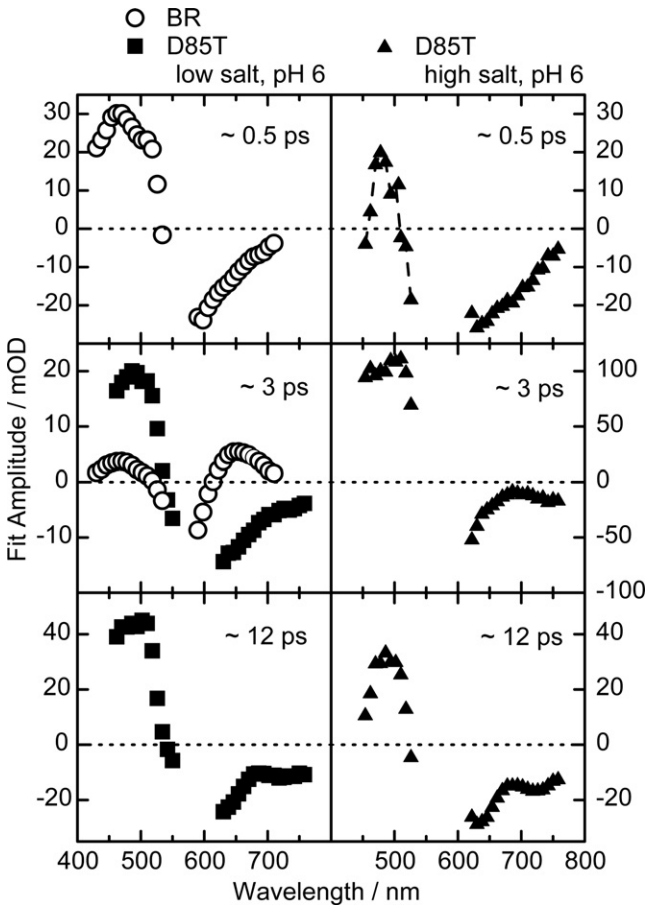

FIGURE 6 Decay-associated spectra of wild-type BR (*open circles*), $D85T_{low\ salt,\ pH\ 6}$ (*squares*), and $D85T_{high\ salt,\ pH\ 6}$ (*triangles*) for the time constants ~0.5 ps, ~3 ps, and ~12 ps. The decay-associated spectra of wild-type BR are scaled by a factor of 0.25.

By taking into account a contribution (25%) of wild-type BR-like behavior, the decay-associated spectrum of the 3 ps kinetic component of $D85T_{high\ salt,\ pH\ 6}$ can be well reproduced from the data of $D85T_{low\ salt,\ pH\ 6}$. We conclude that $D85T_{high\ salt,\ pH\ 6}$ contains a major fraction that exhibits a BR-like behavior with an initial reaction of 0.5 ps.

DISCUSSION

Halorhodopsin

The complete anion transfer in HR at physiological conditions is a multistep process (4) that is initiated by the photoisomerization of the retinal chromophore located in the ion channel. The transient absorption measurements for HR presented above show the same biexponential decay of the excited electronic state, and rather small differences in the time constants for both NaCl concentrations used. Thus, the primary steps in the HR photocycle do not depend on the NaCl concentration. This is somewhat surprising since the function of HR (namely, the pumping of chloride anions into the cytoplasm) strongly depends on the NaCl concentration. Even if one can assume that the occupation of the chloride anion donor site is influenced by the NaCl concentration in the solvent, the transient absorption measurements show that this occupation does not influence the dynamics of the retinal photoisomerization in HR. This finding is also supported by the steady-state absorption studies, in which no effect of the NaCl concentration on the spectral position or shape of the retinal absorption spectrum was found. This means that either the photophysics of the retinal chromophore at the Schiff base of HR is largely independent of the details of the surroundings of the primary donor, or the occupation of the primary anion donor site is not influenced by changes in the NaCl concentration. The concentration of chloride anions is only important for the later steps of the photocycle (33,61).

Mutant D85T

The special properties of the mutant samples can be summarized as follows: The mutation D85T considerably alters the spectral and dynamic behaviors of BR. The pH and salt dependence of the D85T mutant indicates that the samples can be placed into two classes:

1. The three samples ($D85T_{low\ salt,\ pH\ 8}$, $D85T_{high\ salt,\ pH\ 8}$ and $D85T_{low\ salt,\ pH\ 6}$) show a red shift of the peak of the absorption spectrum to ~615 nm. They exhibit a biexponential decay of the excited electronic state with time constants in the 3–12 ps range. The related decay-associated spectra resemble those of HR. However, no chloride pumping activity is found under these conditions.
2. The mutant $D85T_{high\ salt,\ pH\ 6}$ behaves in a different way: its absorption peaks at 570 nm, with a strong red-wing absorption. There is an additional fast-reacting kinetic component (time constant: 0.5 ps) and a (weak) chloride pumping activity (33,62). Qualitatively speaking, this mutant sample behaves as if ~25% of the protein has the absorption spectrum and primary reaction dynamics of native BR. An estimation of the relative isomerization quantum yields for the $D85T_{high\ salt,\ pH\ 6}$ and $D85T_{low\ salt,\ pH\ 6}$ samples of 4:3 was obtained from the transient absorption signals at 678 nm for long delay times. This also is in good agreement with a BR-like contribution of ~25% in the sample.

The inspection of the steady-state absorption spectrum of the $D85T_{high\ salt,\ pH\ 6}$ sample supports this interpretation. The absorption spectrum of $D85T_{high\ salt,\ pH\ 6}$ exhibits signatures for an inhomogeneity. The maximum of the absorption spectrum is located at 570 nm, where the absorption maximum of the wild-type BR is also found. However, this band is much broader than that found for BR, and a distinct shoulder still remains at ~615 nm (Fig. 2). The broad absorption spectrum of $D85T_{high\ salt,\ pH\ 6}$ can be modeled (Fig. 7) by a superposition of the ''typical'' D85T absorption (as seen for the $D85T_{low\ salt,\ pH\ 8}$, $D85T_{high\ salt,\ pH\ 8}$, and $D85T_{low\ salt,\ pH\ 6}$ samples) and the wild-type BR absorption. This indicates that

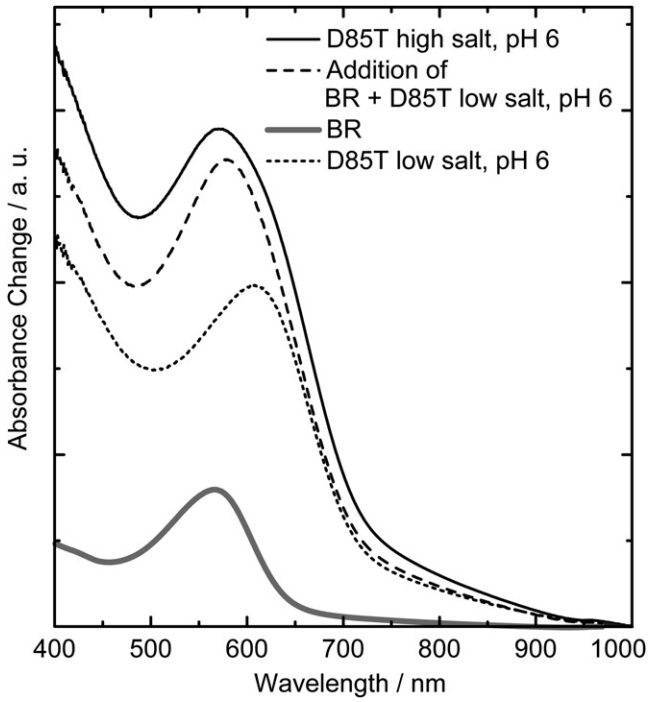

FIGURE 7 Steady-state absorption spectra of BR, $D85T_{low\ salt,\ pH\ 6}$, and $D85T_{high\ salt,\ pH\ 6}$. The combination of the spectra of BR (30%) and $D85T_{low\ salt,\ pH\ 6}$ (70%) reproduces the spectrum of $D85T_{high\ salt,\ pH\ 6}$.

for high NaCl concentration and low pH value (sample $D85T_{high\ salt,\ pH\ 6}$), electrostatic conditions similar to wild-type BR can be achieved for a fraction (estimated to be ~25%) of the $D85T_{high\ salt,\ pH\ 6}$ sample. Apparently, the low pH value and high chloride anion concentration in the $D85T_{high\ salt,\ pH\ 6}$ sample lead to a structural and electrostatic environment for the retinal chromophore for a certain amount (25% of the molecules) that is very similar to the situation found in wild-type BR.

Apart from the spectral and dynamic properties, the transport behavior is also changed for the four D85T samples. Whereas the $D85T_{low\ salt,\ pH\ 8}$, $D85T_{high\ salt,\ pH\ 8}$, and $D85T_{low\ salt,\ pH\ 6}$ samples are inactive transport proteins, the $D85T_{high\ salt,\ pH\ 6}$ sample exhibits a photocycle with active chloride transport. The reactive channel characterized with the time constant of 0.5 ps is responsible for the active transport. This reactive channel is only accessible for 25% of the $D85T_{high\ salt,\ pH\ 6}$. The nonreactive channels are described by time constants of 3 ps and 12 ps, and represent loss channels connected with no ion transport.

In this investigation, three quantities were used to characterize the retinal proteins: 1), the absorption spectrum, which depends on the electrostatics in the surroundings of the retinal chromophore and on the presence and position of the counterion; 2), the primary reaction (isomerization) dynamics, which depends on the potential energy surface and is determined by the steric interactions of the retinal and the electrostatics of the surroundings; and 3), the overall ion pump activity, which is related to the isomerization efficiency, the appropriate counterion, and the properties of the ion transfer channels (as shown in earlier work (31–33)). The behavior of mutant D85T under different buffer conditions might be explained as follows: At high pH values, the aspartic acid D212 in the vicinity of the Schiff base is deprotonated. The associated negative charge causes repulsion of the chloride ion, preventing it from approaching the protonated Schiff base. This explanation is corroborated by the fact that in a previous study of the D85S/D212N double mutation, the pH dependence of anion binding was found to be reduced (35). In additional crystallographic analyses, the protonated Schiff base and the amino acids arginine R82 and aspartate D212 were identified as members of the anion-binding site in the mutant D85S (35). The absence of the Cl^- counterion leads to red-shifted absorption and slow reaction dynamics, and disables the Cl^- pumping activity. For a pH value below the pK_a value of 6.9 for D212 (34), a Cl^- ion could be bound, provided that the Cl^- concentration in the sample is high enough. Thus, a correctly bound Cl^- ion might only occur in the $D85T_{high\ salt,\ pH\ 6}$ sample. If this is indeed the case, the experimental results indicate that the probability that the Cl^- ion position is occupied is ~25% at 1 M NaCl and pH 6.0. The time constant of the initial reaction dynamics of 0.5 ps indicates that these proteins have a potential energy landscape for photoisomerization very similar to that found in wild-type BR. However, slow reaction dynamics are always observed in HR regardless of the concentration of the anion. We therefore conclude that a fundamental difference in the primary reaction kinetics between HR and BR must exist.

In the following, we speculate on three possible explanations for the observed inhomogeneity in the $D85T_{high\ salt,\ pH\ 6}$ sample: 1), a distribution of retinal isomers (all-*trans*, 13-*cis*, and 9-*cis*); 2), the existence of different anion-binding sites; and 3), the incomplete occupation of one binding site.

With respect to the first possibility, extraction experiments performed on all four D85T samples (Table 4) indicate that all samples contain retinal molecules in the all-*trans* and the *cis* form. However, the isomer compositions (Table 4) do not give any indication of the special role of the $D85T_{high\ salt,\ pH\ 6}$ sample. In addition, according to the optical excitation conditions, only the all-*trans* retinal is effectively photoexcited.

As regards the second possibility, in the crystal structure of mutant D85S (which is very similar to D85T (34,35)), only one anion-binding site was found, which was located in the vicinity of the Schiff base (Fig. 8). Thus, the existence of several distinct anion-binding sites is unlikely and cannot be used to explain the observed inhomogeneity.

For the third possibility, we can assume that the Cl^--binding site in HR has been optimized by evolution to also allow its occupation at low NaCl concentrations and nonoptimal pH values. However, one cannot expect the same

TABLE 4 Analysis of retinal isomers

	pH 8		pH 6	
D85T	low salt	high salt	low salt	high salt
illuminated				
all-*trans*	43%	25%	52%	32%
13-*cis*	32%	37%	37%	65%
9-*cis*	25%	38 (44) %	11%	4%
dark-adapted				
all-*trans*	56%	44%	62%	42%
13-*cis*	43%	55%	38%	57%
9-*cis*	1%	<1%	1%	1%

Dark-adapted membranes were suspended in the indicated buffers and kept for 12 h at room temperature in the dark. Illumination was 10 min $\lambda > 515$ nm (the value in parentheses for $D85T_{high\ salt,\ pH\ 8}$ is after illumination with $\lambda > 645$ nm). Values are given in percentage of total retinal.

robustness for the mutated BR protein. Therefore, it is likely that the binding site is not completely occupied under experimental conditions in which the pH value of 6 is close to the pK_a value of the relevant D212.

BR in *H. salinarum* acts as a light-driven proton pump and ensures the photosynthetic activity of the archeon. Thus, BR has been optimized by evolution to transport protons in the most efficient way. On the other hand, HR supports the osmotic balance during cell growth and has a lower quantum yield for the primary reaction. Apparently, the light-induced excitation of HR brings the system into a wide and flat valley in the first electronic potential surface from which different paths can be accessed, but where only one channel leads to the anion pump activity.

Of interest, low-temperature Fourier transform IR studies of D85S(Cl) and HR showed that the hydrogen bond of the protonated Schiff base has similar strengths in D85S(Cl) and BR (63), but not in HR (64). The observed trends in the ultrafast dynamics are similar to those of the hydrogen-bonding strength of the protonated Schiff base. An explanation for this correlation remains to be found.

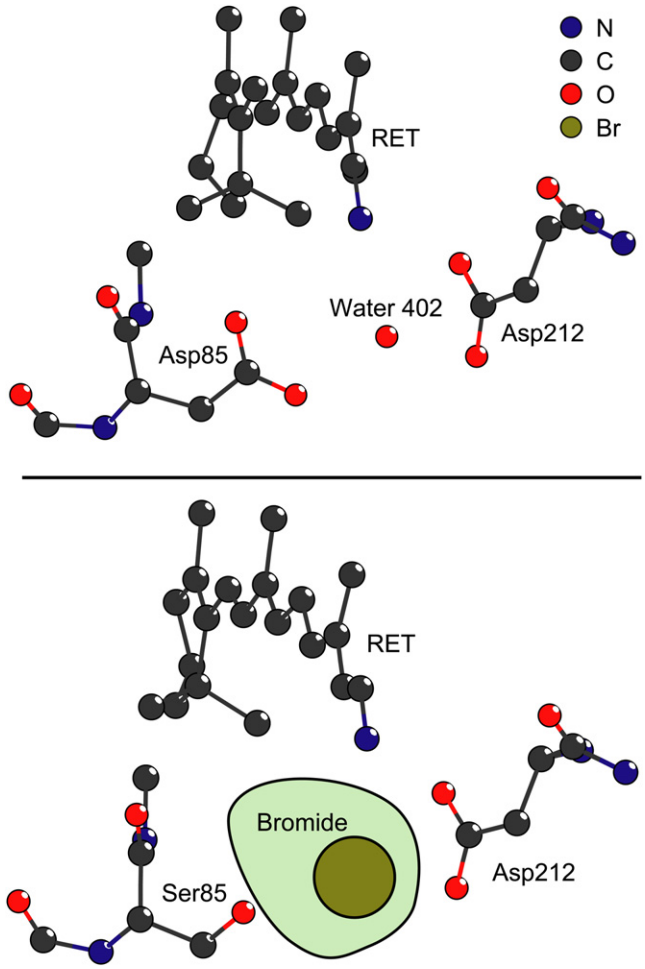

FIGURE 8 Protein structure in the vicinity of the retinal chromophore for wild-type BR (*upper part*) and the mutant D85S (*lower part*). The chromophore retinal (RET) and the amino acids Asp^{212} and Asp^{85} (for BR) or Ser^{85} (for the mutant D85S) are shown. The bromide anion of mutant D85S can be located over a wide area (*light green*). Only with the anion (chloride) in the confined area (*dark green*) are BR-like primary dynamics observed.

CONCLUSIONS

In conclusion, in this study we performed time-resolved transient absorption experiments on femtosecond and picosecond timescales to investigate the initial steps in the primary reaction dynamics of the BR mutant D85T and HR. The experiments on HR show that the primary dynamics and the absorption spectrum are essentially independent of the NaCl concentration in the solvent.

The behavior of the BR mutant D85T (i.e., the absorption spectrum and initial reaction dynamics) depends on environmental parameters such as the pH value and salt concentration. The biexponential reaction dynamics and the range of time constants indicate that the mutation generates a protein with properties similar to those of HR. In the mutant, a modification of the electrostatic environment in the vicinity of the Schiff base can be achieved by changing the pH value and NaCl concentration. A low pH value in combination with a high salt concentration generates a subensemble with a BR-like absorption spectrum and a fast, BR-like primary reaction combined with a Cl^--pumping activity. The experimental findings indicate that the geometrical arrangement of charged groups in the vicinity of the Schiff base in BR is optimized for the highest isomerization yield. Apparently, this is achieved by accurate positioning of the counterion, the negatively charged side group of D85. However, the lack of a covalently bound negative counterion in HR does not allow it to achieve simultaneously the most efficient primary photoisomerization and complete occupation of the anion-binding pocket.

The authors thank Dr. Atlanta Cook for a critical reading the manuscript, and the referee for pointing to interesting correlations of our time-resolved experiments with recent Fourier transform IR studies.

This work was supported by the Deutsche Forschungsgemeinschaft (SFB 533).

REFERENCES

1. Haupts, U., J. Tittor, and D. Oesterhelt. 1999. Closing in on bacteriorhodopsin: progress in understanding the molecule. *Annu. Rev. Biophys. Biomol. Struct.* 28:367–399.
2. Lanyi, J. K., A. Duschl, G. W. Hatfield, K. May, and D. Oesterhelt. 1998. Understanding structure and function in the light-driven proton pump bacteriorhodopsin. *J. Struct. Biol.* 124:164–178.
3. Lanyi, J. K. 2004. Bacteriorhodopsin. *Annu. Rev. Physiol.* 66:665–688.
4. Oesterhelt, D. 1995. Structure and function of halorhodopsin. *Isr. J. Chem.* 35:475–494.
5. Lanyi, J. K. 1986. Halorhodopsin: a light-driven chloride ion pump. *Annu. Rev. Biophys. Biophys. Chem.* 15:11–28.
6. Katre, N. V., P. K. Wolber, W. Stoeckenius, and R. M. Stroud. 1981. Attachment site(s) of retinal in bacteriorhodopsin. *Proc. Natl. Acad. Sci. USA.* 78:4068–4072.
7. Lemke, H. D., and D. Oesterhelt. 1981. Lysine-216 is a binding-site of the retinyl moiety in bacteriorhodopsin. *FEBS Lett.* 128:255–260.
8. Bayley, H., K. S. Huang, R. Radhakrishnan, A. H. Ross, Y. Takagaki, et al. 1981. Site of attachment of retinal in bacteriorhodopsin. *Proc. Natl. Acad. Sci. USA.* 78:2225–2229.
9. Degroot, H. J. M., S. O. Smith, J. Courtin, E. Vandenberg, C. Winkel, et al. 1990. Solid-state C-13 and N-15 NMR study of the low pH forms of bacteriorhodopsin. *Biochemistry.* 29:6873–6883.
10. Trissl, H. W., and M. Montal. 1977. Electrical demonstration of rapid light-induced conformational-changes in bacteriorhodopsin. *Nature.* 266:655–657.
11. Michel, H., and D. Oesterhelt. 1976. Light-induced changes of pH gradient and membrane potential in *H. halobium*. *FEBS Lett.* 65: 175–178.
12. Duschl, A., and G. Wagner. 1986. Primary and secondary chloride transport in *Halobacterium halobium*. *J. Bacteriol.* 168:548–552.
13. Schobert, B., and J. K. Lanyi. 1982. Halorhodopsin is a light-driven chloride pump. *J. Biol. Chem.* 257:10306–10313.
14. Takahashi, T., H. Tomioka, N. Kamo, and Y. Kobatake. 1985. A photosystem other than Ps370 also mediates the negative phototaxis of *Halobacterium halobium*. *FEMS Microbiol. Lett.* 28:161–164.
15. Hazemoto, N., N. Kamo, Y. Terayama, Y. Kobatake, and M. Tsuda. 1983. Photochemistry of 2 rhodopsinlike pigments in bacteriorhodopsin-free mutant of *Halobacterium halobium*. *Biophys. J.* 44:59–64.
16. Bogomolni, R. A., and J. L. Spudich. 1982. Identification of a 3rd rhodopsin-like pigment in phototactic *Halobacterium halobium*. *Proc. Natl. Acad. Sci. USA.* 79:6250–6254.
17. Spudich, J. L., and R. A. Bogomolni. 1984. Mechanism of color discrimination by a bacterial sensory rhodopsin. *Nature.* 312:509–513.
18. Wolff, E. K., R. A. Bogomolni, P. Scherrer, B. Hess, and W. Stoeckenius. 1986. Color discrimination in halobacteria—spectroscopic characterization of a 2nd sensory receptor covering the blue-green region of the spectrum. *Proc. Natl. Acad. Sci. USA.* 83:7272–7276.
19. Luecke, H., B. Schobert, H.-T. Richter, J.-P. Cartailler, and J. K. Lanyi. 1999. Structure of bacteriorhodopsin at 1.55 Å resolution. *J. Mol. Biol.* 291:899–911.
20. Kolbe, M., H. Besir, L.-O. Essen, and D. Oesterhelt. 2000. Structure of the light-driven chloride pump halorhodopsin at 1.8 Å resolution. *Science.* 288:1390–1396.
21. Blanck, A., and D. Oesterhelt. 1987. The halo-opsin gene. II. Sequence, primary structure of halorhodopsin and comparison with bacteriorhodopsin. *EMBO J.* 6:265–273.
22. Mukohata, Y., K. Ihara, T. Tamura, and Y. Sugiyama. 1999. Halobacterial rhodopsins. *J. Biochem. (Tokyo).* 125:649–657.
23. Havelka, W. A., R. Henderson, and D. Oesterhelt. 1995. 3-Dimensional structure of halorhodopsin at 7-Angstrom resolution. *J. Mol. Biol.* 247:726–738.
24. Schreckenbach, T., B. Walckhoff, and D. Oesterhelt. 1977. Studies on retinal-protein interaction in bacteriorhodopsin. *Eur. J. Biochem.* 76:499–511.
25. Kolbe, M. 2001. Röntgenographische und spektroskopische Charakterisierung der lichtgetriebenen Ionenpumpe Halorhodopsin aus Halobacterium salinarum. PhD thesis. Ludwig-Maximilians-Universität München, München, Germany.
26. Khorana, H. G., G. E. Gerber, W. C. Herlihy, C. P. Gray, R. J. Anderegg, et al. 1979. Amino-acid sequence of bacteriorhodopsin. *Proc. Natl. Acad. Sci. USA.* 76:5046–5050.
27. Henderson, R., and P. N. T. Unwin. 1975. 3-Dimensional model of purple membrane obtained by electron-microscopy. *Nature.* 257:28–32.
28. Oesterhelt, D., P. Hegemann, and J. Tittor. 1985. The photocycle of the chloride pump halorhodopsin. 2. Quantum yields and a kinetic model. *EMBO J.* 4:2351–2356.
29. Havelka, W. A., R. Henderson, J. A. W. Heymann, and D. Oesterhelt. 1993. Projection structure of halorhodopsin from *Halobacterium halobium* at 6-Angstrom resolution obtained by electron cryomicroscopy. *J. Mol. Biol.* 234:837–846.
30. Varo, G., L. S. Brown, R. Needleman, and J. K. Lanyi. 1996. Proton transport by halorhodopsin. *Biochemistry.* 35:6604–6611.
31. Tittor, J., U. Schweiger, D. Oesterhelt, and E. Bamberg. 1994. Inversion of proton translocation in bacteriorhodopsin mutants D85N, D85T, and D85,96N. *Biophys. J.* 67:1682–1690.
32. Sasaki, J., L. S. Brown, Y. S. Chon, H. Kandori, A. Maeda, et al. 1995. Conversion of bacteriorhodopsin into a chloride-ion pump. *Science.* 269:73–75.
33. Tittor, J., U. Haupts, C. Haupts, D. Oesterhelt, A. Becker, et al. 1997. Chloride and proton transport in bacteriorhodopsin mutant D85T: different modes of ion translocation in a retinal protein. *J. Mol. Biol.* 271:405–416.
34. Facciotti, M. T., V. S. Cheung, C. S. Lunde, S. Rouhani, N. S. Baliga, et al. 2004. Specificity of anion binding in the substrate pocket of bacteriorhodopsin. *Biochemistry.* 43:4934–4943.
35. Facciotti, M. T., S. Rouhani, and R. M. Glaeser. 2004. Crystal structures of bR(D85S) favor a model of bacteriorhodopsin as a hydroxyl-ion pump. *FEBS Lett.* 564:301–306.
36. Paula, S., J. Tittor, and D. Oesterhelt. 2001. Roles of cytoplasmic arginine and threonine in chloride transport by the bacteriorhodopsin mutant D85T. *Biophys. J.* 80:2386–2395.
37. Dobler, J., W. Zinth, W. Kaiser, and D. Oesterhelt. 1988. Excited-state reaction dynamics of bacteriorhodopsin studied by femtosecond spectroscopy. *Chem. Phys. Lett.* 144:215–220.
38. Atkinson, G. H., T. L. Brack, D. Blanchard, and G. Rumbles. 1989. Picosecond time-resolved resonance raman-spectroscopy of the initial *trans* to *cis* isomerization in the bacteriorhodopsin photocycle. *Chem. Phys.* 131:1–15.
39. Bardeen, C. J., Q. Wang, and C. V. Shank. 1998. Femtosecond chirped pulse excitation of vibrational wave packets in LD690 and bacteriorhodopsin. *J. Phys. Chem. A.* 102:2759–2766.
40. Kahan, A., O. Nahmias, N. Friedman, M. Sheves, and S. Ruhman. 2007. Following photoinduced dynamics in bacteriorhodopsin with 7-fs impulsive vibrational spectroscopy. *J. Am. Chem. Soc.* 129: 537–546.
41. Nuss, M. C., W. Zinth, W. Kaiser, E. Kölling, and D. Oesterhelt. 1985. Femtosecond spectroscopy of the first events of the photochemical cycle in bacteriorhodopsin. *Chem. Phys. Lett.* 117:1–7.
42. Polland, H.-J., M. A. Franz, W. Zinth, W. Kaiser, E. Kölling, et al. 1986. Early picosecond events in the photocycle of bacteriorhodopsin. *Biophys. J.* 49:651–662.
43. Mathies, R., C. Cruz, W. Pollard, and C. Shank. 1988. Direct observation of the femtosecond excited-state *cis-trans* isomerisation in bacteriorhodopsin. *Science.* 240:777–779.
44. Butt, H. J., K. Fendler, E. Bamberg, J. Tittor, and D. Oesterhelt. 1989. Aspartic acid-96 and aspartic acid-85 play a central role in the function of bacteriorhodopsin as a proton pump. *EMBO J.* 8:1657–1663.

45. Thorgeirsson, T. E., S. J. Milder, L. J. W. Miercke, M. C. Betlach, R. F. Shand, et al. 1991. Effects of Asp-96-Asn, Asp-85-Asn, and Arg-82-Gln single-site substitutions on the photocycle of bacteriorhodopsin. *Biochemistry*. 30:9133–9142.

46. Fahmy, K., O. Weidlich, M. Engelhard, J. Tittor, D. Oesterhelt, et al. 1992. Identification of the proton acceptor of Schiff-base deprotonation in bacteriorhodopsin—a Fourier-transform-infrared study of the mutant Asp85-Glu in its natural lipid environment. *Photochem. Photobiol.* 56:1073–1083.

47. Metz, G., F. Siebert, and M. Engelhard. 1992. Asp(85) is the only internal aspartic acid that gets protonated in the M-intermediate and the purple-to-blue transition of bacteriorhodopsin—a solid-state C-13 CP-MAS NMR investigation. *FEBS Lett.* 303:237–241.

48. Polland, H.-J., M. A. Franz, W. Zinth, W. Kaiser, P. Hegemann, et al. 1985. Picosecond events in the photochemical cycle of the light-driven chloride-pump halorhodopsin. *Biophys. J.* 47:55–59.

49. Peters, F., J. Herbst, J. Tittor, D. Oesterhelt, and R. Diller. 2006. Primary reaction dynamics of halorhodopsin, observed by sub-picosecond IR vibrational spectroscopy. *Chem. Phys.* 323:109–116.

50. Arlt, T., S. Schmidt, W. Zinth, U. Haupts, and D. Oesterhelt. 1995. The initial reaction dynamics of the light-driven chloride pump halorhodopsin. *Chem. Phys. Lett.* 241:559–565.

51. Kandori, H., K. Yoshihara, H. Tomioka, and H. Sasabe. 1992. Primary photochemical events in halorhodopsin studied by subpicosecond time-resolved spectroscopy. *J. Phys. Chem.* 96:6066–6071.

52. Nakamura, T., S. Takeuchi, M. Shibata, M. Demura, H. Kandori, et al. 2008. Ultrafast pump-probe study of the primary photoreaction process in pharaonis halorhodopsin: halide ion dependence and isomerization dynamics. *J. Phys. Chem. B.* 112:12795–12800.

53. Satzger, H., C. Root, C. Renner, R. Behrendt, L. Moroder, et al. 2004. Picosecond dynamics in water soluble azobenzene-peptides. *Chem. Phys. Lett.* 396:191–197.

54. Schmidt, B., C. Sobotta, B. Heinz, S. Laimgruber, M. Braun, et al. 2005. Excited-state dynamics of bacteriorhodopsin probed by broadband femtosecond fluorescence spectroscopy. *Biochim. Biophys. Acta.* 1706:165–173.

55. Huber, R., H. Satzger, W. Zinth, and J. Wachtveitl. 2001. Noncollinear optical parametric amplifiers with output parameters improved by the application of a white light continuum generated in CaF2. *Opt. Commun.* 194:443–448.

56. Seel, M., E. Wildermuth, and W. Zinth. 1997. A multichannel detection system for application in ultra-fast spectroscopy. *Meas. Sci. Technol.* 8:449–452.

57. Oesterhelt, D., and W. Stoeckenius. 1974. Isolation of the cell membrane of *Halobacterium halobium* and its fractionation into red and purple membrane. *Methods Enzymol.* 31:667–678.

58. Heymann, J. A. W., W. A. Havelka, and D. Oesterhelt. 1993. Homologous overexpression of a light-driven anion pump in an archaebacterium. *Mol. Microbiol.* 7:623–630.

59. Pfeiffer, M., T. Rink, K. Gerwert, D. Oesterhelt, and H. J. Steinhoff. 1999. Site-directed spin-labeling reveals the orientation of the amino acid side-chains in the E-F loop of bacteriorhodopsin. *J. Mol. Biol.* 287:163–171.

60. Fischer, U. C., P. Towner, and D. Oesterhelt. 1981. Light-induced isomerization, at acidic pH, initiates hydrolysis of bacteriorhodopsin to bacterio-opsin and 9-*cis*-retinal. *Photochem. Photobiol.* 33:529–537.

61. Haupts, U., J. Tittor, E. Bamberg, and D. Oesterhelt. 1997. General concept for ion translocation by halobacterial retinal proteins: the isomerization/switch/transfer (IST) model. *Biochemistry*. 36:2–7.

62. Tittor, J., D. Oesterhelt, and E. Bamberg. 1995. Bacteriorhodopsin mutants D85n, D85t and D85,96n as proton pumps. *Biophys. Chem.* 56:153–157.

63. Shibata, M., K. Ihara, and H. Kandori. 2006. Hydrogen-bonding interaction of the protonated Schiff base with halides in a chloride-pumping bacteriorhodopsin mutant. *Biochemistry*. 45:10633–10640.

64. Shibata, M., N. Muneda, T. Sasaki, K. Shimono, N. Kamo, et al. 2005. Hydrogen-bonding alterations of the protonated Schiff base and water molecule in the chloride pump of. *Natronobacterium pharaonis*. 44:12279–12286.